# PROPOSAL OF NUMERICAL WAVE FLUME FOR WAVE OVERTOPPING COMPUTATION CONSIDERING WIND EXTERNAL FORCE

Masami Kiku[1] and Koji Kawasaki[2]

Strong wind blows around seawalls when wave overtopping disasters occur. Consequently, wind effects on wave overtopping are essential in designing seawalls. However, the relationship between wind and wave overtopping rate has not been clarified quantitatively because it is difficult to estimate the wind effects by hydraulic model experiments. The objective of this study was to introduce wind external force to a two-dimensional numerical model based on a numerical wave flume 'CADMAS-SURF'. A TimerDoor method, which was a computational method for the motion of water particles and air bubbles, was improved to represent wind-induced acceleration motion. The proposed method was validated through comparison with hydraulic model experiments. As a result, the dimensionless wave overtopping rates obtained by the numerical computations were in reasonable agreement with the experimental results. It was found that the proposed model is useful for wave overtopping simulation considering wind effects.

*Keywords: wave overtopping; wind external force; CADMAS-SURF; numerical simulation; wave deformation; irregular wave*

## INTRODUCTION

Japan often experiences natural disasters caused by typhoons. Among them, wave overtopping disaster is a serious problem because a lot of major roads have been developed along coastal lines. Wave overtopping disasters, such as the destruction of seawalls and traffic interruption, have occurred in recent years. Therefore, sufficient countermeasures against the wave overtopping have not been taken.

Wave overtopping phenomena are affected by various factors. One of important factors is wind around seawalls. When a typhoon approaches and passes over a seawall, it generates a strong wind around the seawall. Therefore, it is essential to consider the effects of the wind in estimating the wave overtopping discharge. Attempts to clarify the effects of wind on the wave overtopping phenomenon have been made primarily through hydraulic model experiments performed in a wind-wave tunnel (e.g., Iwagaki et al. 1965, Takada 1976), and the results indicate the importance of considering the effects of wind in estimating the overtopping discharge. However, the law of similarity for converting the experimental wind velocity to the field wind speed, in general, has a limitation for application of the experimental results in the field. Yamashiro et al. (2004) showed from comparison with the field observations that a calibration value for converting the wind velocity of a hydraulic model experiment using a 1:45 scale model into the field wind speed was approximately one-third. However, they mentioned that the use of the calibration value is limited because of the dependence on the scale of the experiment. Pullen et al. (2009) proposed a wind transport factor $f_{\mathrm{wind}}$ based on field observations as a method to obtain the mean overtopping discharge including wind $q_{\mathrm{wind}}$. The proposed equation was based on limited observational data from Europe. Hence, its applicability to near-shore areas around Japan is unclear because the conditions for wave growth are different. In response to the results of the existing studies, Goda (2008) expressed a view that although the effects of wind are greater for lower wave overtopping rate, no quantitative evaluation methods have been established. In spite of the numerous investigations performed on the relationship between the wind speed and wave overtopping discharges, there are few findings applicable to seawall design. Additionally, the effects of wind on the overtopping discharges are rarely considered.

Recently, wave overtopping computations using a numerical model have been increasingly applied to seawall design. The numerical computation can be applied to phenomena corresponding to different scales. Hence, it is extremely advantage for seawall design if the effects of wind on wave overtopping discharges can be analyzed at the field scale. Various numerical models dealing with both air and water motion have ever been developed. It is considered appropriate to apply a single-phase model capable of dynamically solving the interaction between the air and water for the wave overtopping simulation with wind. However, it would require a considerable amount of computational time to satisfy the CFL (Courant Friedrichs Lewy) conditions in the two-phase model compared with the one-phase model because the flow velocity of air become easily larger than that of water. This currently makes it

[1] Department of Civil Engineering, Nagoya University, Furo-cho, Chikusa-ku, Nagoya 464-8603, Japan
[2] Hydro-soft Technology Institute Co., Ltd., 3-3-23, Nakanoshima, Kita-Ku, Osaka 530-6126 Japan

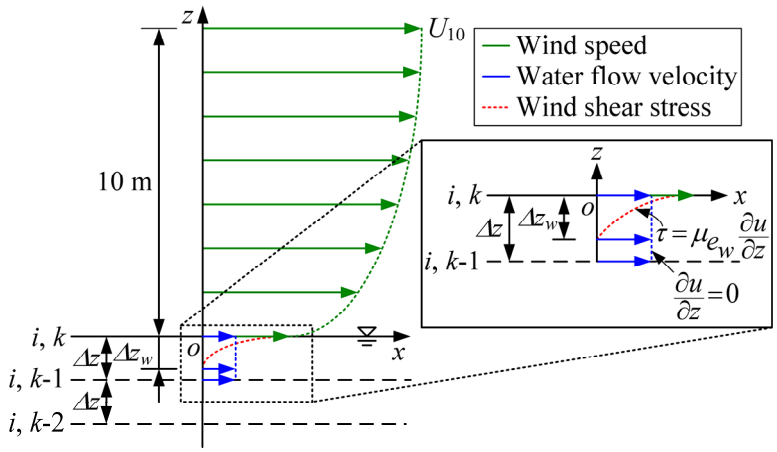


**Figure 1. Modeling of sea surface shearing stress.**

impractical to use the two-phase model for simulation of the wave overtopping considering wind. On the other hand, a two-dimensional cross-sectional numerical wave flume, CADMAS-SURF (SUper Roller Flume for Computer Aided Design of MAritime Structures; Coastal Development Institute of Technology, 2001; Coastal Development Institute of Technology, 2008), has showed reasonable results in the wave overtopping simulation that uses a single-phase model. If computation of wave overtopping phenomena considering wind external force becomes possible with CADMAS-SURF, it would be useful for designing seawalls.

From these background and motivation, this study proposes a wave overtopping analysis method that can consider wind external force based on the numerical wave flume CADMAS-SURF. Additionally, the study examines the validity of the proposed method by numerically simulating wave overtopping phenomena in the previous hydraulic model experiment considering wind.

## IMPLEMENTATION OF WIND EXTERNAL FORCE TO NUMERICAL WAVE FLUME 'CADMAS-SURF'

Wind affects the overtopping discharge through two actions: wave deformation in front of the seawall, and the transportation of the water particles behind the seawall. This chapter proposes a method of incorporating these two actions into CADMAS-SURF.

### Implementation of wind shear stress to free surface

This study considers the horizontal component of the wind vector, and models the wind shear stress generated on the sea surface by sea wind as shown in Figure 1. Assuming that the vertical distribution of the sea wind follows the logarithmic law, the wind shear stress $\tau$ acting on the sea surface is typically estimated by Eq. (1). This estimation utilizes the wind speed $U_{10}$ at an elevation of 10 m above sea level and the sea surface drag coefficient $C_{DO}$. The thickness of vertical layer of the fluid affected by the wind shear stress $\tau$, which acts on the sea surface, is defined as $\Delta z_w$. Accordingly, the shear stress $\tau$, between the sea surface and $\Delta z_w$, is expressed as Eq. (2). By discretizing Eq. (2) using Eq. (1), horizontal velocity $u_k$ of the free surface with the application of wind shear stress can be expressed as Eq. (3).

$$\tau = \rho_a C_{DO} {U_{10}}^2 \tag{1}$$

$$\tau = \mu_{e_w} \frac{\partial u}{\partial z} \tag{2}$$

$$u_k = u_{z_w} + \frac{\Delta z_w}{\nu_{e_w} \rho_w} \rho_a C_{DO} {U_{10}}^2 \tag{3}$$

where $\rho_a$ and $\rho_w$ are the densities of air and water, respectively, $\mu_{e_w}$ and $\nu_{e_w}$ are the coefficient of viscosity and dynamic coefficient of viscosity in $\Delta z_w$, respectively. Further, $u_{z_w}$ is the horizontal

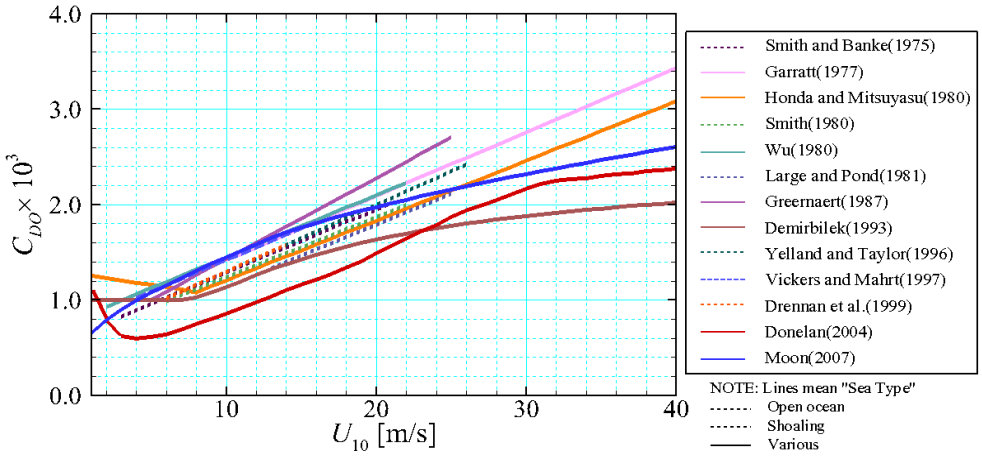


**Figure 2. Comparison of various surface drag coefficients.**

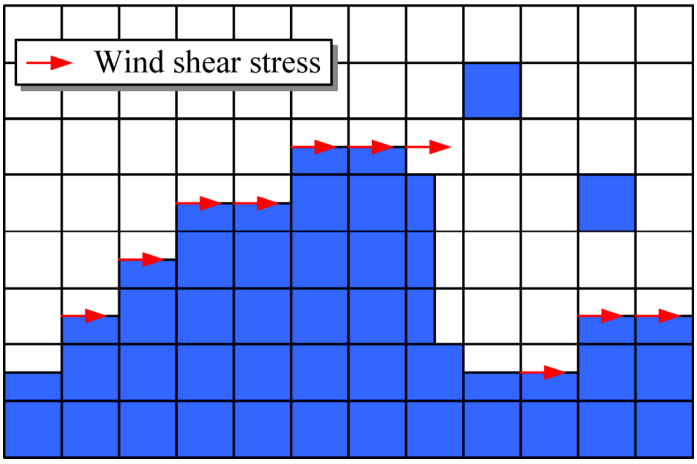


**Figure 3. Conceptual diagram of the wind shear stress applied to CADMAS-SURF.**

velocity at $z = z_w$. In this analysis, $\Delta z_w$ was set at 0.01 m, which is a constant based on the results of trial tests with varying values of $\Delta z_w$. Various empirical equations have been proposed for the sea surface drag coefficient $C_{DO}$, which are derived from field observations, theories, and laboratory and numerical experiments. Figure 2 shows comparison of various surface drag coefficients, which have been ever proposed. From this figure, this study adopted the equation proposed by Donelan et al. (2004) because this curve was described on various conditions.

Figure 3 shows the conceptual diagram of the wind shear stress applied to CADMAS-SURF. As stated earlier, Eq. (3) was assumed to be defined when the wind and sea surface were parallel to each other. Additionally, the wind shear stress was applied only to the cells whose free surface was perpendicular to the $z$-axis and wherein the fluid existed in the negative direction of the $z$-axis. However, the wind shear stress was not assumed to act on the downwind side of the wave crest. The wind shear stress was applied only to the surface cells on the upwind side based on the spatial gradient of the VOF (Volume of Fluid) function $F$, which was computed using Eq. (4).

$$-\frac{(F_{i,k} - F_{i,k-1})/\Delta z}{(F_{i,k} - F_{i-1,k})/\Delta x} > 0 \qquad (4)$$

where $\Delta x$ and $\Delta z$ are the horizontal and vertical grid sizes, respectively, and $F$ is the VOF function which expresses full cell, surface cell and empty cell for $F = 1.0$, $0.0 < F < 1.0$ and $F = 0.0$, respectively.

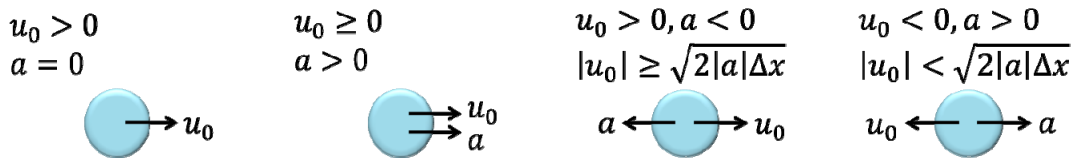


(a) Type 1 (b) Type 2 (c) Type 3 (d) Type 4

**Figure 4. Water particle motion pattern in the horizontal (positive) direction.**

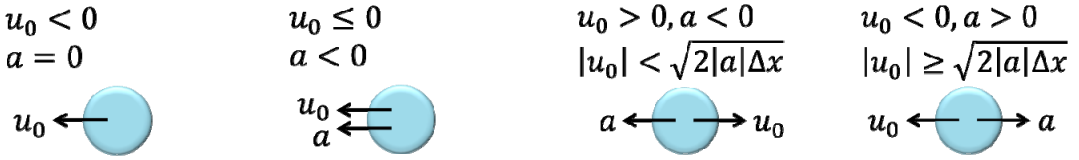


(a) Type 1 (b) Type 2 (c) Type 3 (d) Type 4

**Figure 5. Water particle motion pattern in the horizontal (negative) direction.**

The area considering wind external force can be specified such that the wind external force acts from the upwind side, according to the relationship between the distance $x$ from the wave generating position and generation time $t$.

**Acceleration of water particles through wind external force**

As CADMAS-SURF is a single-phase model, it cannot use directly the behaviors of air bubbles in the water or water particles in air that are generated during wave breaking or wave overtopping. The computation becomes unstable by these air bubbles and water particles. A TimerDoor method was proposed in CADMAS-SURF to process the water particles and air bubbles simply and appropriately. The TimerDoor method separated the water particle motion into uniform (horizontal direction) and free-fall (vertical direction) motions based on the initial velocity of a particle. Next, the time $t'$ for the water particle to move to the next cell was calculated and the water particle was moved to the next cell after $t'$.

When wind acts on the water particles, horizontal motion of water particles must be calculated as acceleration motion. The horizontal motion of the water particle was modified from the existing uniform motion to acceleration. This was done to simulate through CADMAS-SURF the wind action transporting the water particle over the seawall to its rear face. The water particle's mass $m$ and drag $D$ with respect to the wind can be obtained from Eqs. (5) and (6), respectively. Therefore, the water particle's horizontal acceleration $a$, generated by the wind speed $U$, is computed using Eq. (7).

$$m = \Delta x \cdot \Delta z \cdot F \cdot \rho_w \tag{5}$$

$$D = 0.5 \cdot \rho_w \cdot (U - u_0)^2 C_{DW} \cdot \Delta z \tag{6}$$

$$a = D / m \tag{7}$$

where $u_0$ is the initial speed of the water particle in the horizontal direction and $C_{DW}$ is the drag coefficient of the particle with respect to the wind.

Based on the relationship between $a$ and $u_0$ of the water particles obtained from the equations above, the horizontal motions of a particle are categorized into eight patterns in two horizontal (positive and negative) directions as shown in Figures 4 and 5. Further, by computing the transit time $t'$ to the next cell in each pattern, and moving the particle after $t'$, the acceleration of the wind-affected particle can be represented.

Figure 6 shows the comparison of the analytical and simulated results when a water particle is placed at $x$ = 2.5 m and $z$ = 4.5 m. The drag coefficient of the particle $C_{DW}$ was set at 1.0 in this case. In

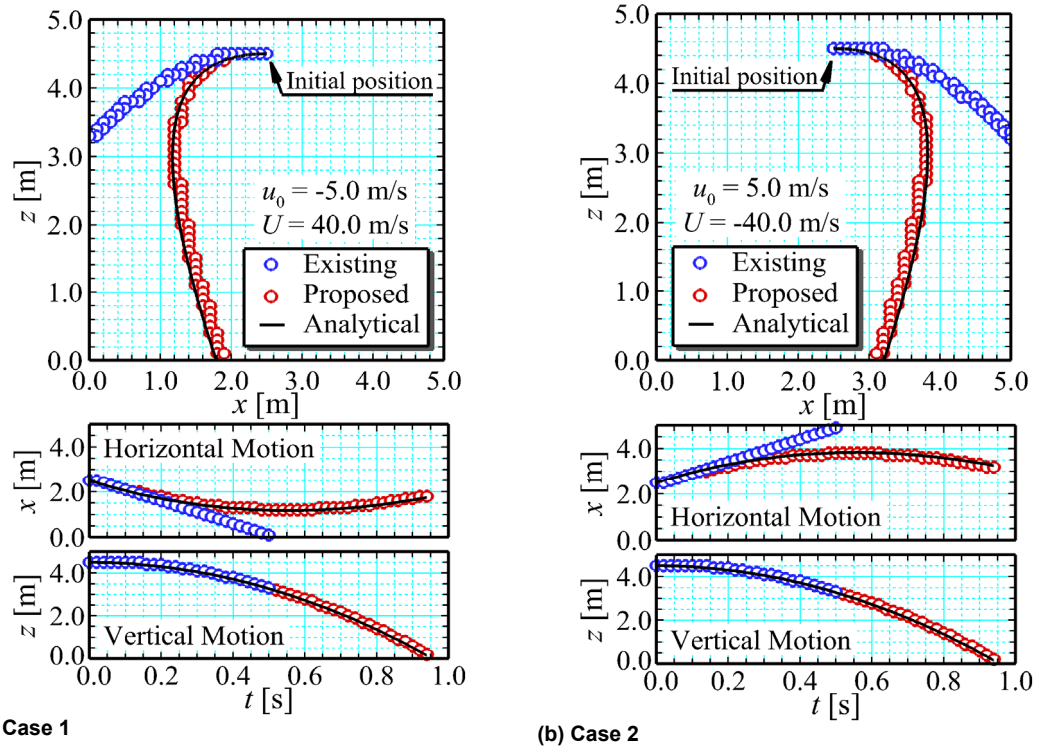


**(a) Case 1** **(b) Case 2**

**Figure 6. Validity as compared with the acceleration of the water particles.**

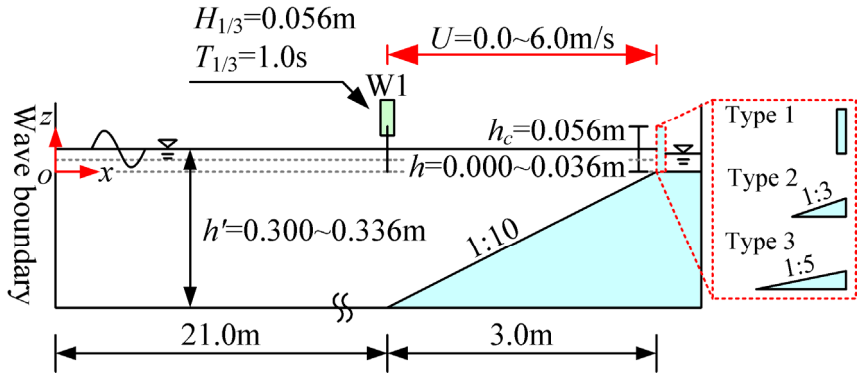


**Figure 7. Schematic of computational setup.**

this figure, a black line shows analytical results and blue circles and red circles indicate existing and proposed results, respectively. Figure 6(a) shows the simulation results, with an initial speed in the horizontal direction of $u_0$ = -5.0 m/s and wind speed of $U$ = 40.0 m/s. From this figure, the particle moved in the negative direction from the initial position and subsequently turned to move in the positive direction after $t$ = 0.6 s due to the positive wind speed. On the other hand, in Figure 6(b), under the conditions $u_0$ = 5.0 m/s and $U$ = -40.0 m/s, the motion of the particle changed toward the negative direction after $t$ = 0.6 s. The simulation results in both the cases are closely consistent with the analytical result. Hence, the particle motion under the wind action, which was not calculated using the existing method, was determined to be appropriately expressed. Only the horizontal component of wind was reconsidered for the particle motion. The vertical motion was processed as a free fall according to conventional methods.

## VALIDITY OF THE PROPOSED NUMERICAL WAVE FLUME

The proposed method is validated through comparison with hydraulic model experiments conducted by Inoue et al. (1992).

| Table 1. Wave conditions. | |
|---|---|
| Spectrum type | Bretschneider - Mitsuyasu |
| Significant wave height $H_{1/3}$ | 0.056 m |
| Significant wave period $T_{1/3}$ | 1.0 s |
| Wave steepness $(H/L)_{1/3}$ | 0.04 |
| Relative crown height $h_c/H_{1/3}$ | 1.0 |
| Relative water depth $h/L_{1/3}$ | 0.000, 0.013, 0.026 |
| Non-dimensional wind speed $U/\sqrt{gH_{1/3}}$ | 0, 4, 8 |
| Drag coefficient of the particle $C_{DW}$ | 0.4, 0.7, 1.0, 1.4 |

| Table 2. Computational parameters. | | |
|---|---|---|
| Simulation time | Simulation interval $\Delta t$ | $10^{-8}$ – $10^{-3}$ s |
| | Simulation end $t_{END}$ | 250 s |
| Method of wave generation | Wave model | Wave boundary |
| | No. of wave components | 200 |
| | No. of vertical division | 29 |
| | Initial random number | 5963 |
| Grid size | x-direction $\Delta x$ | 0.0125 – 0.0200 m |
| | z-direction $\Delta z$ | 0.0090 – 0.0200 m |
| Difference scheme | DONOR parameter | VP-DONOR0.2 |
| Boundary conditions | Velocity and pressure | Slip |
| | VOF function $F$ | Free |

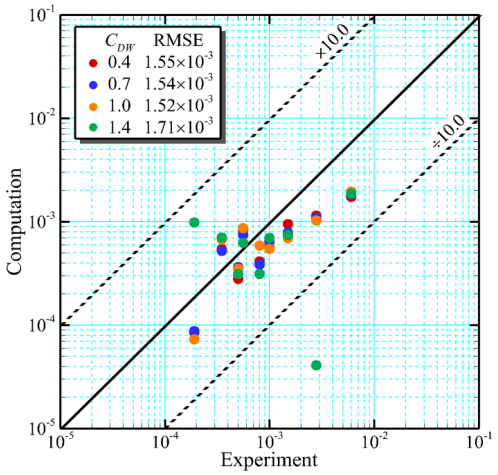


**Figure 8. Dimensionless wave overtopping rate.**

### Simulation parameters and analytical methods

The schematic of the computational setup is shown in Figure 7. Tables 1 and 2 show the wave conditions and computational parameters, respectively. A uniform slope of 1:10 originating at $x = 21.0$ m was positioned in the flume. Three shapes of the seawall, vertical (Type 1), 1:3 slope (Type 2), and 1:5 slope (Type 3) were chosen. They were placed such that the relative crown height $h_c/H_{1/3}$ was 1.0. Irregular incident waves in the shape of the Bretschneider-Mitsuyasu spectrum were generated at $x = 0.0$ m using wave boundary. The incident waves were calibrated, resulting in a significant wave height $H_{1/3}$ and significant wave period $T_{1/3}$ were 0.056 m and 1.0 s, respectively, at the wave height gauge point W1 shown in Figure 7. Inoue et al. (1992) did not refer to the number of components, incident waveform, and wave generation time of the irregular wave. An irregular wave signal was generated with 200 wave components and an initial random value of 5963, as described in Table 2. The simulation period was set at 250 s and the data recording starting at 86.16 s, when the wave became stabilized sufficiently. This resulted in an analysis running of 163.84 s. The wind speed $U$ was set to various speeds of 0.0, 3.0, and 6.0 m/s. Wind was blown from the $x = 21.0$ m point in the hydraulic model experiment. Accordingly, in this computation, the range for application of the wind shear stress and the computational domain of the particle acceleration were also set from $x = 21.0$ m to the seawall. The results of the experiment by Inoue et al. (1992) were summarized by using the wind speed 0.24 m above the crown of the seawall as the representative wind speed. The proposed method

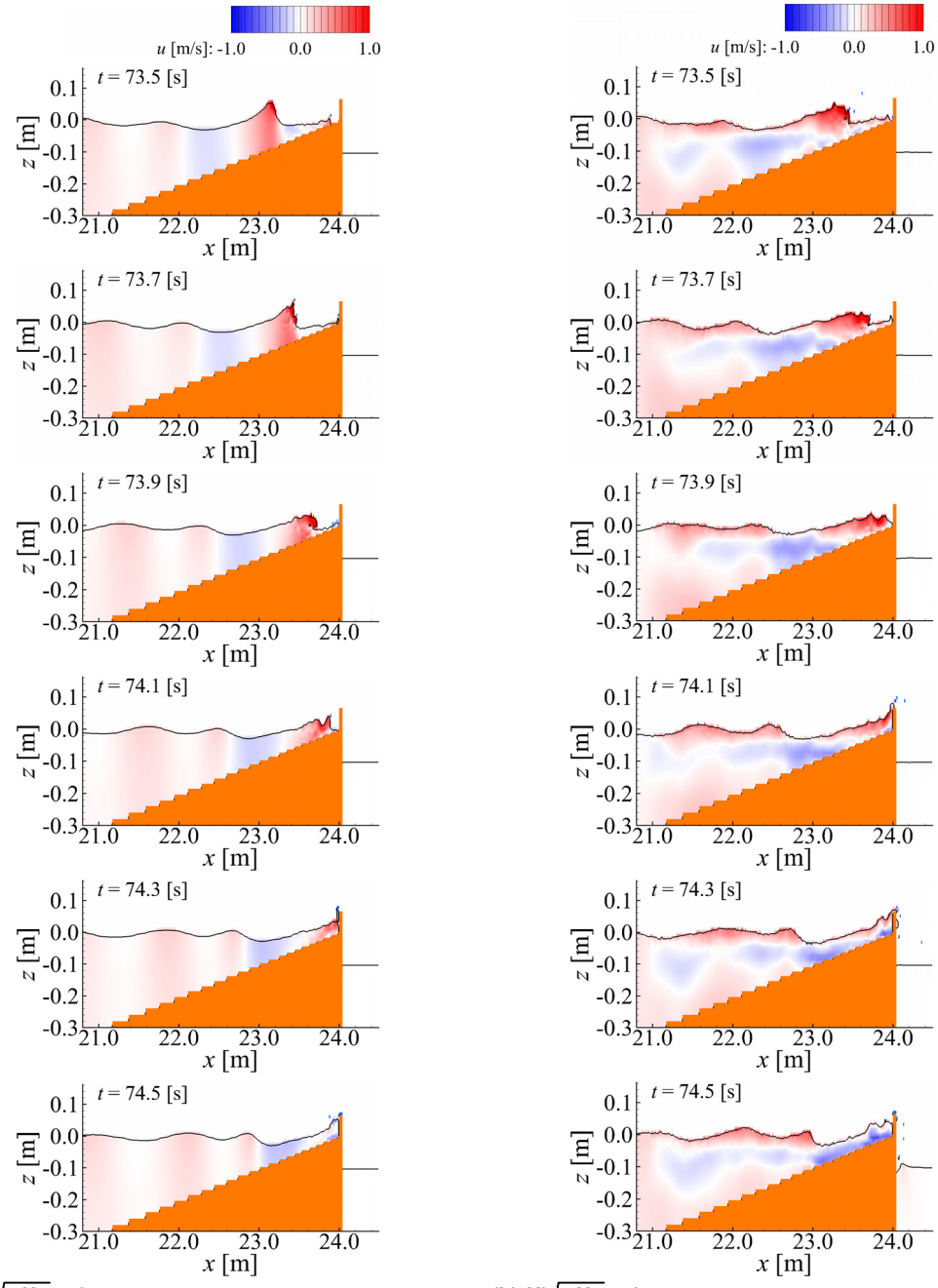


**(a)** $U/\sqrt{gH_{1/3}} = 0$ **(b)** $U/\sqrt{gH_{1/3}} = 8$

**Figure 9. Change in water surface surrounding the vertical seawall ($h/L_{1/3} = 0.000$).**

assumes the mean wind speed profile to be logarithmic. Hence, the wind speed at the height of 0.24 m above the crown of the seawall was assumed to be approximately equal to the wind speed $U_{10}$ at the height of 10 m above the crown of the seawall. In addition, the same wind speed used in the hydraulic model experiment was input in the numerical simulation.

Irregularly spaced grids, which were finest on the free surface and around the structure, were applied in the computational domain. This was done to analyze the wave deformation and wave overtopping phenomena with high accuracy and efficiency. A wave overtopping pit area was provided behind the seawall. A time series of the change in overtopping discharges was obtained from the area integral of the VOF function $F$ value. Further, the overtopping rate $q$ was computed by dividing the total overtopping discharges by the analysis time (163.84 s).

A trial tests were carried out to investigate the optimum drag coefficient of the particle $C_{DW}$ under no wind and the relative water depths $h/L_{1/3} = 0.000$, 0.013 and 0.026. Figure 8 shows dimensionless

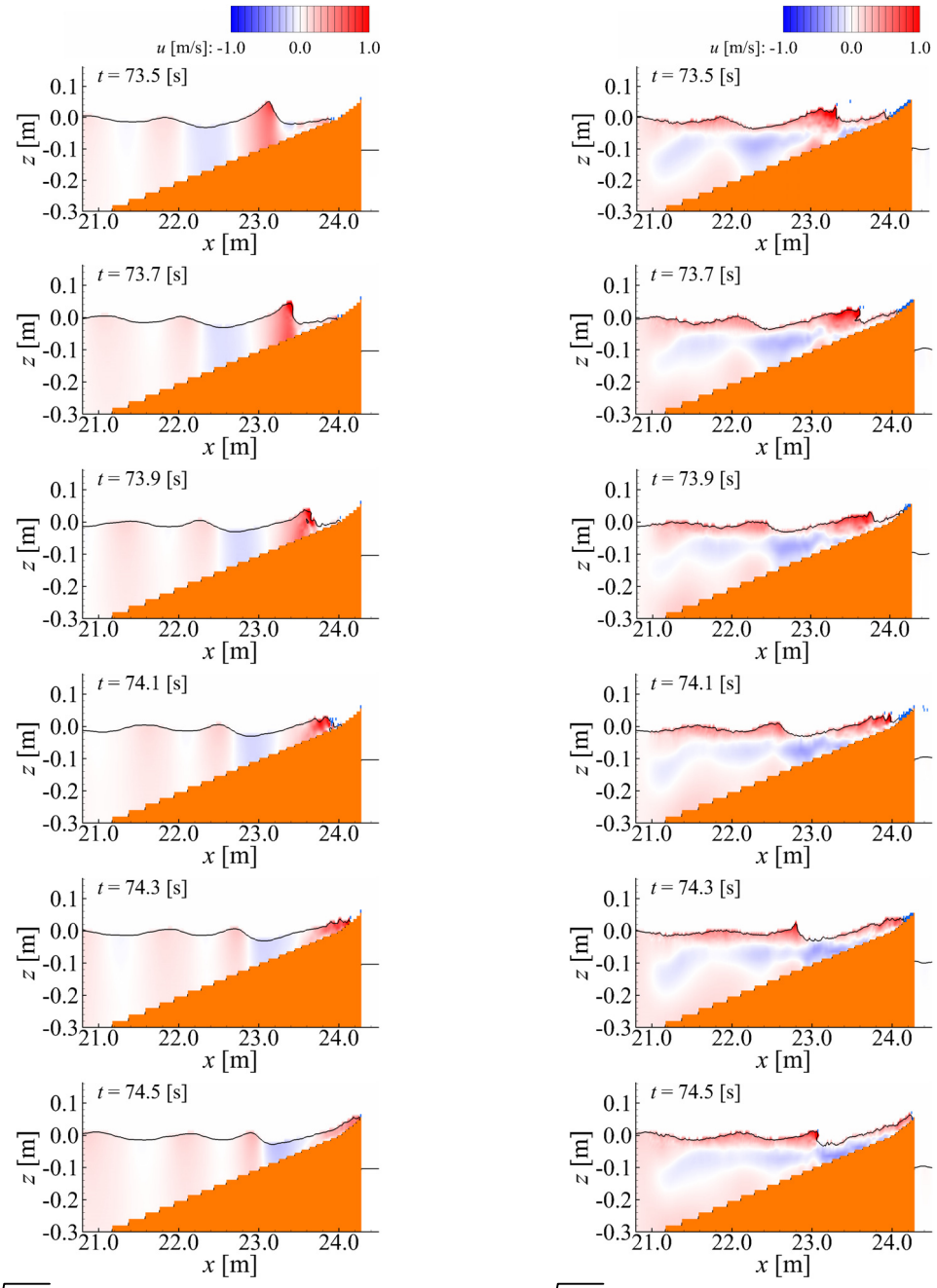


**(a) $U/\sqrt{gH_{1/3}} = 0$** **(b) $U/\sqrt{gH_{1/3}} = 8$**

**Figure 10. Change in water surface surrounding the 1:5 slope seawall ($h/L_{1/3} = 0.000$).**

wave overtopping rate of experimental and computational results. From this figure, almost numerical computational results underestimate wave overtopping rate of experimental results. However, the computational results are found to be estimate the experimental results in the range of same order except for the case of $C_{DW} = 1.4$. In this study, $C_{DW} = 1.0$ was determined because RMS (root mean square) becomes minimum value.

### The effects of wind external force on wave deformation on seaward face of seawall

Figures 9 and 10 show examples of the spatial profile of the water surface around the vertical and 1:5 slope seawalls. Figure 9(a) shows the spatial profile of the water surface surrounding the vertical seawall without wind. The figure shows that the incident wave was elevated on the slope face as the water became shallower, and it broke at approximately $x = 23.2$ m. After that, wave height dissipated and overtopped at $t = 74.3$ s. However, as shown in Figure 9(b), when the value of non-dimensional

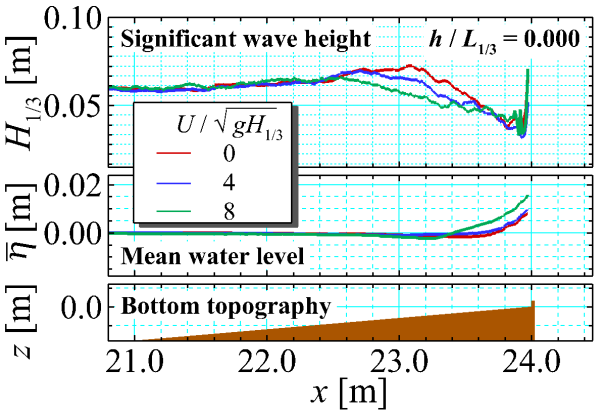


**(a) $h/L_{1/3}$ = 0.000**

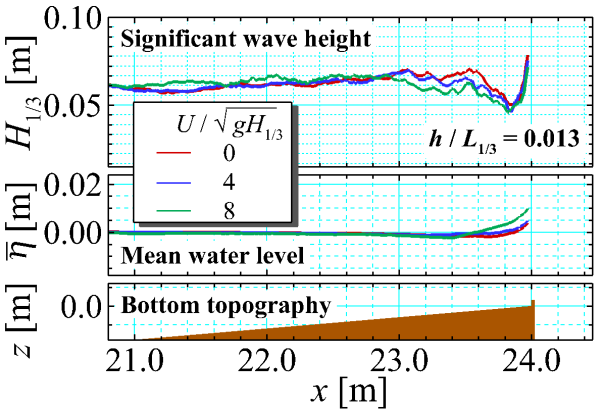


**(b) $h/L_{1/3}$ = 0.013**

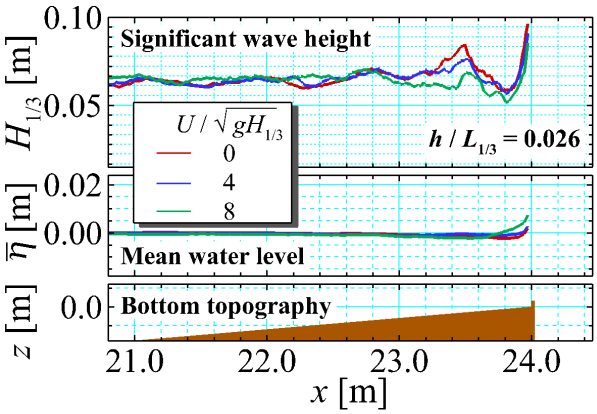


**(c) $h/L_{1/3}$ = 0.026**

**Figure 11. Spatial distribution of significant wave height and mean water level with respect to vertical seawall.**

wind speed $U/\sqrt{gH_{1/3}}$ was 8, the wave breaking and overtopping had already occurred at $t$ = 73.5 s and $t$ = 74.1 s , respectively. Moreover, short period waves were generated on the free surface at $U/\sqrt{gH_{1/3}}$ = 8. Additionally, Figures 9(b) and 10(b) show that the landward horizontal flow velocity $u$ was higher at the non-dimensional wind speed $U/\sqrt{gH_{1/3}}$ = 8 than that with no wind. They also show that a seaward horizontal flow velocity developed near the bottom surface as return flow for the landward current generated near the free surface. These results qualitatively demonstrate the effectiveness of applying the wind shear stress to the free surface in the proposed computational method.

At the non-dimensional wind speed $U/\sqrt{gH_{1/3}}$, the wave deformation, such as the difference in breaking point and an increase in mean water level, on the seaward face of the seawall can also be

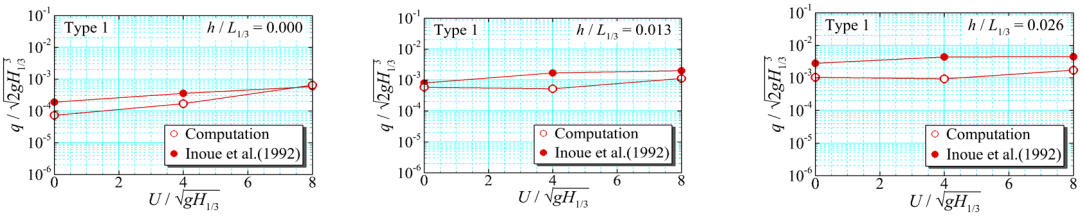


**(a) $h/L_{1/3}$ = 0.000** **(b) $h/L_{1/3}$ = 0.013** **(c) $h/L_{1/3}$ = 0.026**

**Figure 12. Relationship between non-dimensional wind speeds and overtopping discharges for vertical seawall.**

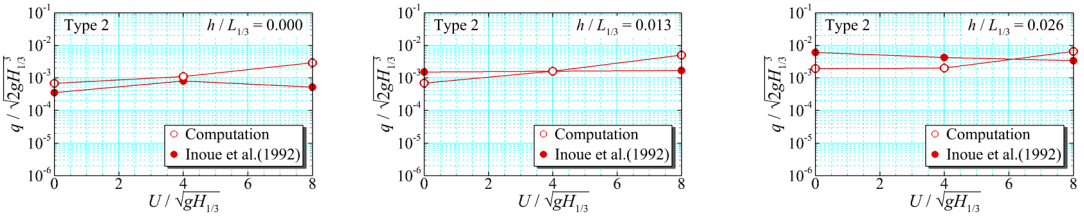


**(a) $h/L_{1/3}$ = 0.000** **(b) $h/L_{1/3}$ = 0.013** **(c) $h/L_{1/3}$ = 0.026**

**Figure 13. Relationship between non-dimensional wind speeds and overtopping discharges for 1:3 slope seawall.**

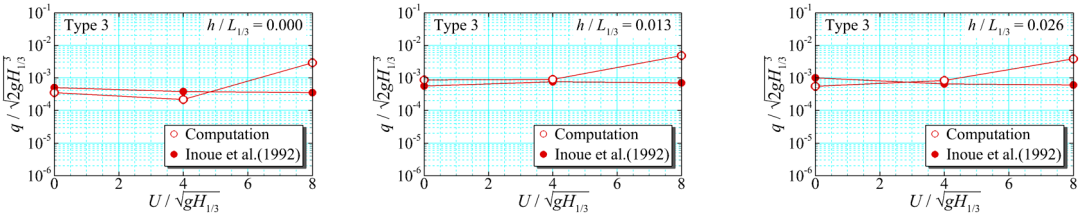


**(a) $h/L_{1/3}$ = 0.000** **(b) $h/L_{1/3}$ = 0.013** **(c) $h/L_{1/3}$ = 0.026**

**Figure 14. Relationship between non-dimensional wind speeds and overtopping discharges for 1:5 slope seawall**

observed quantitatively from Figure 11. The figure shows the spatial distribution of significant wave height $H_{1/3}$ and mean water level $\overline{\eta}$. It is clear from the spatial distribution of $H_{1/3}$ shown in Figure 11(a) that the wave breaking point moved seaward as $U/\sqrt{gH_{1/3}}$ increased. With reference to the wave deformation induced by wind on the seaward face of the seawall, Nagai and Ueda (1960) have stated that the wave breaks farther seaward under windy conditions compared to the condition when there is no wind. This is because the wave crest is pushed by the wind pressure. The same phenomenon was confirmed using the proposed method. Thus, it was qualitatively showed that the computation considering the wind external force was appropriately executed. The spatial distribution of $\overline{\eta}$, as shown in Figure 11(a), shows that $\overline{\eta}$ on the seaward face of the seawall increased significantly with the increase in $U/\sqrt{gH_{1/3}}$. This indicates not only the wave setup due to the wave breaking but also the wind setup at the seawall. These tendencies were also clear at different relative water depths $h/L_{1/3}$, as shown in Figures 11(b) and (c). However, when $U/\sqrt{gH_{1/3}}$ was the same value, the decrease in $h/L_{1/3}$ pushed the wave breaking point farther seaward and $\overline{\eta}$ higher. The characteristics of the spatial distributions of $H_{1/3}$ and $\overline{\eta}$ with respect to $U/\sqrt{gH_{1/3}}$ and $h/L_{1/3}$ showed approximately the same trends for 1:3 and 1:5 slope seawalls.

**Change in wave overtopping rate over seawall due to wind external force**

Figures 12–14 show the relationship between the non-dimensional wind speed $U/\sqrt{gH_{1/3}}$ and the dimensionless wave overtopping rate $q/\sqrt{2gH_{1/3}^3}$ of the respective seawalls with reference to the relative water depth $h/L_{1/3}$. As shown in Figure 12, the numerical computation for the case of the vertical seawall showed that $q/\sqrt{2gH_{1/3}^3}$ increased with the increase in $U/\sqrt{gH_{1/3}}$. This agrees with the trend in the hydraulic model experiment performed by Inoue et al. (1992), who concluded that the

overtopping rate over the vertical seawall is easily susceptible to the effects of wind. The numerical simulation also accurately computed $q/\sqrt{2gH_{1/3}^3}$ of the hydraulic model experiment when $U/\sqrt{gH_{1/3}}$ was 0 and 4 for 1:3 slope and 1:5 slope seawalls, respectively, as shown in Figures 13 and 14. However, $q/\sqrt{2gH_{1/3}^3}$ was maximum at $U/\sqrt{gH_{1/3}} = 8$ in all simulation cases for the sloped seawalls. With reference to the case of wave overtopping considering wind near the gently sloped seawall, Inoue et al. (1992) stated that although the waves broken on the uniform slope face rise up as a splash, they fall on the sloping face of the seawall before reaching the rear of the seawall. Thus, wave overtopping does not occur. However, according to the numerical computation, the probability of wave overtopping is assumed to be higher in the presence of wind than without it. This is because the mean water level $\overline{\eta}$ on the seaward face of the seawall increases with the increase in $U/\sqrt{gH_{1/3}}$. The reason for this is considered to be that the wind external force at $U/\sqrt{gH_{1/3}} = 8$ is overestimated in the numerical computation. As described earlier, the definition of the incident wave profile, wave generation time, and overtopping rate of the irregular wave were different from those in the hydraulic model experiment. Thus, the wave conditions considering wind on the seaward face of the seawall require further analysis. However, based on the results of the numerical simulation considering wind, $q/\sqrt{2gH_{1/3}^3}$ is of a similar order as the results of the hydraulic model experiment. Therefore, in the low $U/\sqrt{gH_{1/3}}$ range, the proposed numerical wave flume is observed to satisfactorily simulate the dimensionless wave overtopping rate.

## CONCLUSIONS

This study proposed a method to apply a wind external force to a two-dimensional numerical wave flume CADMAS-SURF to investigate the effects of wind on the overtopping rate. In addition, it examined the validity of the proposed computational method based on a comparison with the previous hydraulic model experiment. As a result, it was determined that the proposed computational method was applicable to the analysis of wave overtopping over seawalls considering wind external force. Although the proposed computational method in this study is simple, it enables field scale analyses and the quantitative evaluation of the effect of overtopping rate considering wind, which was difficult in hydraulic model experiments. Therefore, this method would be helpful in the design of seawalls that prevent wave overtopping. Future improvement is required, as this study did not consider wind speeds in the vertical direction. The thickness $\Delta z_w$ of vertical layer affected by the wind shear stress, and drag coefficient $C_{DW}$, were set based on the results of the trial tests in this study. However, further analysis is necessary through comparison with hydraulic model experiments and similar investigations.

## ACKNOWLEDGMENTS

The authors would like to express their appreciation for the partial funding of this study by the Grant-in-Aid for Young Scientists (A) (principal investigator: Masami Kiku, Nagoya University, project number: 26709035) and the Funds for the Development of Human Resources in Science and Technology (principal investigator: Masami Kiku, Nagoya University, project number: 2110250).

## REFERENCES

Coastal Development Institute of Technology. 2001. *Research and development on numerical wave flume (CADMAS-SURF) report on application of numerical wave flume to wave resistant design*, Coastal Development Technology Library, No. 12, 457 p. (in Japanese).

Coastal Development Institute of Technology. 2008. *Collection of actual CADMAS-SURF simulation examples- interim report on application of numerical wave tank to wave resistant design*, Coastal Development Technology Library, No. 30, 368 p. (in Japanese).

Demirbilek, Z., S. M. Bratos, and E. F. Thompson. 1993. Wind products for use in coastal wave and surge models, *U.S. Army Engineer Waterways Experiment Station*, Coastal Engineering Research Center, Miscellameous Report CERC-93-7.

Donelan, M. A., B. K. Haus, N. Reul, W. J. Plant, M. Stiassnie, H. C. Graber, O. B. Brown and E. S. Saltzman. 2004. On the limiting aerodynamic roughness of the ocean in very strong winds, *Geophys. Res. Lett.*, Vol. 31, L18306.

Drennan, W. M., K. K. Kahma, and M. A. Donelan. 1999. On momentum flux and velocity spectra over waves, *Boundary-Layer Meteorology*, Vol. 92, 3, pp. 489–515.

Garratt, J. R. 1977. Review of drag coefficients over oceans and continents, *Monthly Weather Review*, Vol. 105, 7, pp. 915–929.

Geernaert, G.L. 1987.: On the importance of the drag coefficient in air-sea interactions, *Dynamics of Atmospheres and Oceans*, Vol. 11, 1, pp. 19–38.

Goda, Y. 2008. *Wave resistant design of harbor and coastal structures*, Kajima Institute Publishing Co., Ltd., pp. 430.

Honda, T. and H. Mitsuyasu. 1980. Experimental research of effect of wind on water surface, *Proceedings of Coastal Engineering*, JSCE, Vol. 27, pp. 90–93 (in Japanese).

Inoue, M., H. Shimada, and H. Enma. 1992. Wind effects on characteristics of wave overtopping over mild slope seawall, *Proceedings of Coastal Engineering*, JSCE, Vol. 39, pp. 586–590 (in Japanese).

Iwagaki, Y., M. Inoue, and K. Ohori. 1965. Studies on the effect of wind on wave overtopping on seawalls (second report), *Proceedings of Coastal Engineering*, JSCE, Vol. 12, pp. 168–192 (in Japanese).

Large, W. G. and S. Pond. 1981. Open ocean momentum flux measurements in moderate to strong winds, *Journal of Physical Oceanography*, Vol. 11, 3, pp. 324–336.

Moon, I. J., I. Ginis, T. Hara, and B. Thomas. 2007. A physics-based parameterization of air-sea momentum flux at high wind speeds and its impact on hurricane intensity predictions, Monthly Weather Review, Vol. 135, 8, pp. 2869–2878.

Nagai, S., and S. Ueda. 1960. Study on the shape and structure of seawall considering wind and waves, *Proceedings of Coastal Engineering*, JSCE, Vol, 7, pp. 245–273 (in Japanese).

Pullen, T., W. Allsop, T. Bruce, and J. Pearson. 2009. Field and laboratory measurements of mean overtopping discharges and spatial distributions at vertical seawalls, *Coastal Engineering*, Vol. 56, 2, pp. 121–140.

Reul, N., H. Branger, and J. P. Giovanangeli. 1999. Air flow separation over unsteady breaking waves, *Physics of Fluids*, Vol. 11, 7, pp. 1959-1961.

Smith, S. D. 1980. Wind stress and heat flux over the ocean in gale force winds, *Journal of Physical Oceanography*, Vol. 10, 5, pp. 709–726.

Smith, S. D. and E. G. Banke. 1975. Variation of the sea surface drag coefficient with wind speed, *Q.J.R. Meteorol. Soc.*, Vol. 101, 429, pp. 665–673.

Takada, A. 1976. Wind effect on the overtopping discharges of regular waves, *Proceedings of Coastal Engineering*, JSCE, Vol. 23, pp. 170–175 (in Japanese).

Vickers, D. and L. Mahrt. 1997. Fetch limited drag coefficients, *Boundary-Layer Meteorology*, Vol. 85, 1, pp. 53–79.

Wu, J. 1980. Wind-stress coefficients over sea surface near neutral conditions -a revisit, *Journal of Physical Oceanography*, Vol. 10, 5, pp. 727–740.

Yamashiro, M., A. Yoshida, H. Hashimoto, N. Kurushima, and I. Irie. 2004. Conversion of the wind velocity in wave-overtopping experiment into the wind velocity of the real coast, *Proceedings of Civil Engineering in the Ocean*, JSCE, Vol. 20, pp. 653–658 (in Japanese).

Yelland, M. and P. K. Taylor. 1996. Wind stress measurements from the open ocean, *Journal of Physical Oceanography*, Vol. 26, 4, pp. 541–558.